# Vibrational spectra of dense, hydrous magnesium silicates at high pressure: Importance of the hydrogen bond angle

## A.M. HOFMEISTER,[1,*] H. CYNN,[2] P.C. BURNLEY,[3] AND C. MEADE[4]

[1]Department of Earth and Planetary Sciences, Washington University, St. Louis, Missouri 63130, U.S.A.
[2]Lawrence Livermore National Laboratories, Livermore, California 94550, U.S.A.
[3]Department of Geology, Georgia State University, Atlanta, Georgia 30303, U.S.A.
[4]Geophysical Laboratory, 5251 Broad Branch Road, N.W., Washington, D.C. 20015, U.S.A.

## ABSTRACT

Changes in configuration and hydrogen bonding are inferred from the complex responses of peak parameters (frequency, width, height, and area) to compression for various hydroxyl groups in dense, hydrous magnesium silicates (DHMS). Stretching frequencies ($\nu_i$) depend not only on both O-H...O bond length but also bond angle, which suggests a need to re-examine frequency-structure relationships at 1 atm. For phase B [$Mg_{12}{}^{VI}Si^{IV}Si_3O_{19}(OH)_2$], $\nu$ of the most intense $OH^-$ peak determined from IR spectra at nearly hydrostatic pressures ($P$) decreases to a minimum at 5 GPa, and then rises to a broad maximum near 35 GPa, whereas $\nu$ of the other intense peak decreases to a broad minimum near 30 GPa. This behavior shows that compression of phase B initially moves O19 toward H2 on O21 and rotates H1 about O20 away from O19 and toward O21 inside the triangle of O atoms, thus increasing the H1-O20-O19 bond angle (from 12 to 21° at 37 GPa). H-H repulsion rotates H2 outside of the triangle by 11° at 37 GPa. Changes in O-O bond length and H-O-O angle calculated from the trends of OH frequency with increasing pressure are consistent with the relatively incompressible layer of $SiO_4$ tetrahedra. Widths, areas, and heights of the hydroxyl peaks also increase with $P$ (whereas areas of the lattice modes are constant), with H1 being much more affected: This response suggests that the H1 bond bends further with compression. Raman spectra of stoichiometric $OH^-$ modes in superhydrous phase B [$Mg_{10}{}^{VI}Si^{IV}Si_2O_{14}(OH)_4$] roughly parallel these trends, consistent with similarly paired hydroxyls with bent bonds. For phase A [$Mg_7{}^{IV}Si_2O_8(OH)_6$], the Raman $OH^-$ bands depend linearly on $P$, and with constant peak height with slopes similar to those observed for weak stretching modes of trace H in phase B. This behavior is common and is associated with linear hydrogen bonds and unpaired $OH^-$ groups. Combining our data with previous results reveals systematic, linear relationships of $d\nu/dP|_{i0}$ with $\nu$ that suggest high-polyhedral bulk moduli for DHMS.

Most frequencies of 31 mid-IR lattice modes for phase B depend linearly on curvature is seen for several modes. Raman frequencies of lattice modes from superhydrous phase B (shyB) and phase A depend linearly on $P$.

## INTRODUCTION

Hydrogen, if present in the Earth's mantle, affects basic properties such as rheology and processes such as melting and, therefore, the stability of hydrous phases at high pressure and temperature is of great interest (e.g., Luth 1993). A significant number of dense hydrous magnesium silicates are stable near 20 GPa (cf. Prewitt and Finger 1992). The structural role of H is difficult to determine directly through X-ray diffraction (XRD): Thus, complementary information provided by spectroscopy on speciation, concentration, and bonding of H are essential. Several dense, hydrous magnesium silicates (DHMS) have been characterized at 1 atm by infrared (IR) and Raman spectroscopy (Cynn et al. 1996 and references therein), and by nuclear magnetic resonance (NMR) methods (Phillips et al. 1997). Also, some spectra have been obtained at $P$ or at temperature (Williams 1992; Faust and Williams 1996; Liu et al. 1997a, 1997b).

This study presents nearly hydrostatic thin-film infrared absorption spectra of phase B and Raman spectra of phase A and superhydrous phase B (shyB) at pressure. Changes in the peak parameters of the OH bands with $P$ depend crucially on the OH…O bond distance and angle: The importance of the latter parameter was heretofore unrecognized, mainly because systematic studies were performed at 1 atm (e.g., Mikenda 1986).

## EXPERIMENTAL METHODS

Samples were synthesized using the USSA-2000 uniaxial split sphere apparatus in the Center for High Pressure Research, SUNY, Stony Brook as described by Burnley and Navrotsky (1996). Phases were characterized by powder XRD and electron microprobe analyses. Grains of phase B, ~5–10 μm across, were taken from a synthesis at 12 GPa and 1154 °C that also contained olivine and chondrite (the latter was below the XRD detection limit). Grains of shyB, ~100–400 μm across, were taken from a run at 16 GPa and 1172 °C that contained some

phase A and phase E. Grains of phase A, ~100 μm across, were taken from a run at 10 GPa and 1038 °C that contained minor periclase, brucite, and chondrodite.

IR spectra were collected from thin-films made by crushing grains in a diamond-anvil cell (DAC) with type II diamonds. Crushing forms an aggregate of randomly oriented microscopic particles and thus averages the polarizations. Absorption measurements were acquired at 2 cm⁻¹ resolution and 0.01 cm⁻¹ accuracy from ~450 to 5000 cm⁻¹ with an evacuated Fourier transform infrared Bomem DA3.02 spectrometer, a Globar source, a KBr beam splitter, and a liquid nitrogen cooled HgCdTe detector. A stainless steel gasket indented and drilled with ~200 μm diameter holes formed the sample chamber. A film with thickness <0.1 μm was compressed in cryogenically loaded $N_2$ to study the lattice modes. A thicker, ~1 μm, film was compressed in Ar to examine the weak O-H stretching modes. Pressure was determined using the fluorescence of ruby. See Cynn and Hofmeister (1994) for procedural details.

Although IR peaks are commonly fit with a combination of Gaussian and Lorentzian functions, this is not supported by Maxwell's equations (Wooten 1972). Fourier deconvolution (e.g., Kauppinen et al. 1981) assumes that all peaks have the same widths, which is untrue for IR spectra of solids. Therefore, ν was determined directly from the spectra. Peak widths, full width at half maximum (FWHM), and heights were determined utilizing linear baselines. Areas were obtained by integration.

Raman spectra were recorded at the Geophysical Laboratory with a multichannel Raman microprobe (Dilor XY) in a backscattering configuration using a charge-couple device detector with $1024 \times 298$ channels, an Ar⁺ laser, and a Leitz L25 objective. Data were accumulated for 10 min. Peak positions were determined by inspection. Spectra at 1 atm were collected from samples on a glass slide. Pressure measurements were made as above, except that no pressure medium was used. Duffy et al. (1995) give procedural details.

## SYMMETRY ANALYSIS

Phase B and the *Pnnm* space group for shyB (Pacalo and Parise 1992) have different symmetries for IR and Raman modes; however, the frequencies should be similar because mode types (e.g., O-Si-O bending) are duplicated between symmetries (Cynn et al. 1996). For the *P2₁nm* space group for shyB (Kudoh et al. 1994), IR modes are Raman active (Cynn et al. 1996), as occurs for phase A (Table 1). For such cases (e.g., quartz, Scott and Porto 1967), the intense Raman modes should occur at the transverse optic (TO) positions, which lie near the absorption peaks, and extra, weak Raman peaks should equal the longitudinal optic (LO) positions.

Regarding M-O-H bending modes, if the site has axial symmetry about the O-H vector (a linear O-H…O configuration), then only one doubly degenerate bending peak should exist. However, if axial symmetry is lacking (the hydrogen bond is bent), then the in- and out-of-plane bending motions should have different frequencies.

## RESULTS

### Lattice modes at high pressure

**Phase B.** IR peak heights obtained for phase B using liquid $N_2$ as a pressure medium (Fig. 1) change continuously with respect

**TABLE 1.** Symmetry analysis of Phase A, $Mg_7{}^{IV}Si_2O_8(OH)_6$

| Site or type | A*† | B | $E_1$*† | $E_2$† |
|---|---|---|---|---|
| Si2, O6‡ | 2 | 2 | 2 | 2 |
| Si1, Mg3, O5§ | 3 | 3 | 3 | 3 |
| Mg1, Mg2, O1-O4‖ | 18 | 18 | 18 | 18 |
| H1, H2‖ | 6 | 6 | 6 | 6 |
| Total | 29 | 29 | 29 | 29 |
| **Type determined by Factor Group Analysis** | | | | |
| Acoustic | 1 | | 1 | |
| Symmetric Si-O stretch | 1 | 1 | 1 | 1 |
| Symmetric O-Si-O bend | 2 | 2 | 2 | 2 |
| Asymmetric Si-O stretch | 3 | 3 | 3 | 3 |
| Asymmetric O-Si-O bend | 3 | 3 | 3 | 3 |
| $SiO_4$ librations | 3 | 3 | 3 | 3 |
| $SiO_4$ translations | 2 | 3 | 2 | 3 |
| O2-Mg3-O4 bend# | 6 | 6 | 6 | 6 |
| Mg1, Mg2 translations# | 2 | 2 | 2 | 2 |
| O-H stretch | 2 | 2 | 2 | 2 |
| Mg-O-H bend | 4 | 4 | 4 | 4 |

*Notes:* Structure $P6_3 = C_6^6$ and $Z = 2$ (Horiuchi et al. 1979). Total number of vibrations is 174. The acoustic modes are active in the Raman but not the IR. Because the Raman and the IR spectra share the same symmetries, both LO and TO components will be Raman-active. The factor group analysis considers only the TO modes (the LO modes will have the same assignment) and assumes no accidental degeneracies.
*Raman active.
†Infrared active.
‡ The site is a in Wycoff notation and the symmetry is $C_3(2)$ for each atom.
§The site is b in Wycoff notation and the symmetry is $C_3(2)$ for each atom.
‖The site is c in Wycoff notation and the symmetery is $C_1(6)$ for each atom.
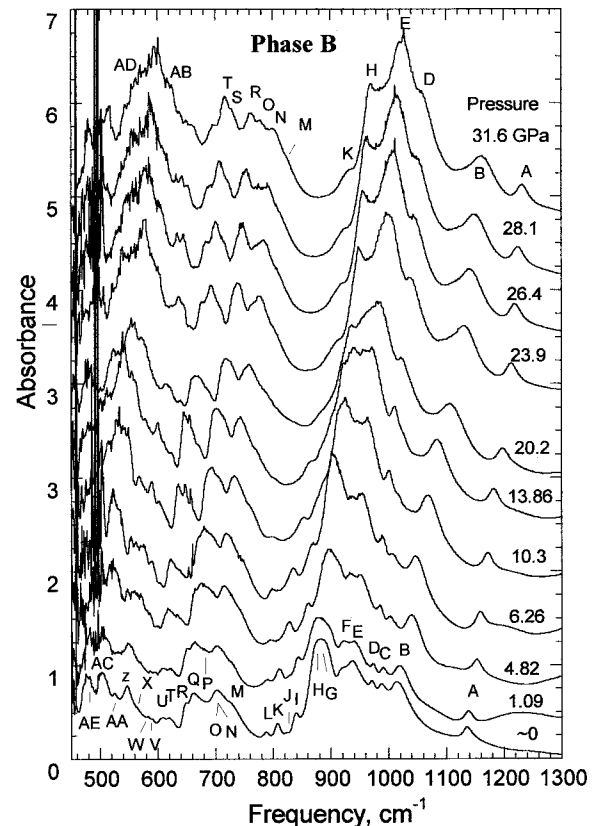#The number of modes is approximate, but the sum of both types is 8 in each symmetry.



**FIGURE 1.** Selected mid-IR spectra of phase B from the $N_2$ runs. Lattice modes are labeled alphabetically with reference to Table 2. Pressures are given on the right hand side. Each spectrum above 1 atm was offset sequentially by increments of 0.5 absorbance units for clarity.
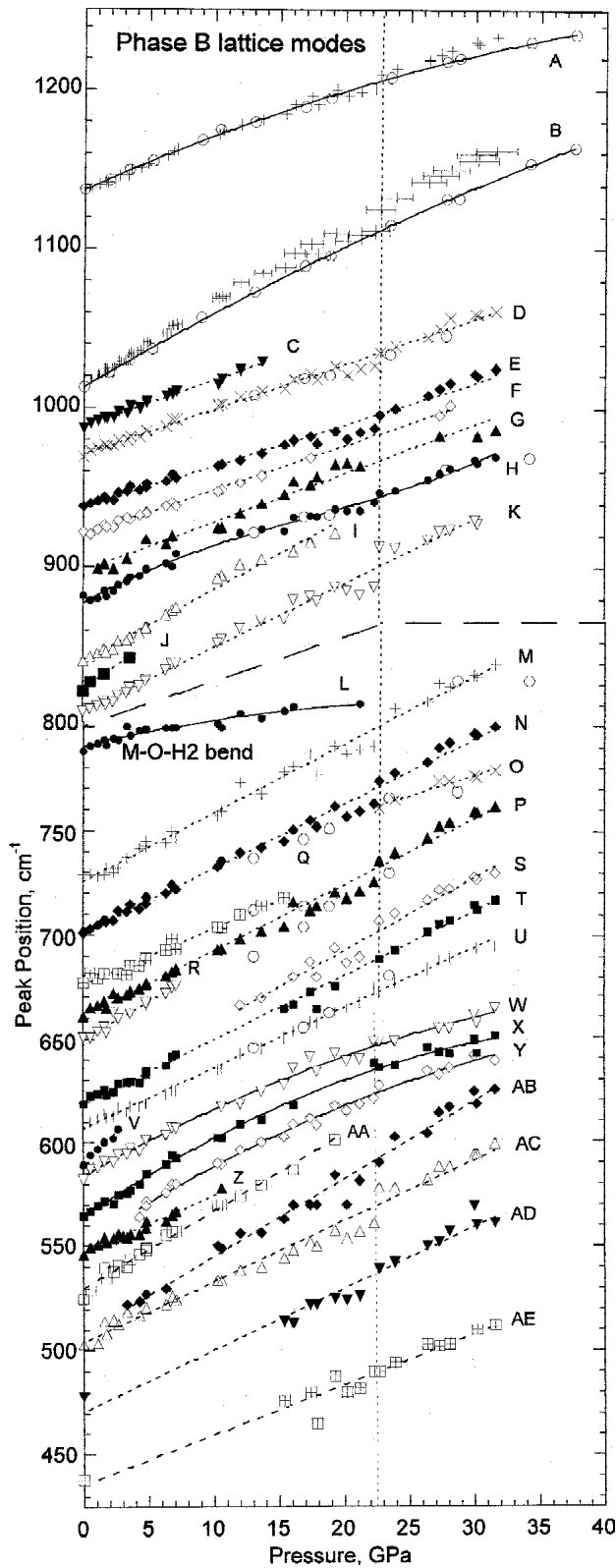
FIGURE 2. Dependence of the IR lattice modes of phase B on pressure. Labels A–Z, AA–AE key this plot to Figure 1 and Table 2. The y axis scale differs above and below 800 cm⁻¹. A phase transition might occur at 22.5 GPa, as indicated by the vertical dashed line. Open circles, experiments from a thick sample in Ar; all other symbols are from the thin sample in N₂. Solid lines quadratic or cubic least-squares fits of with P. Dashed or dotted lines, linear least-squares fits of with P. Error bars are shown for the peak initially at 1013 cm⁻¹. The undulation in peak H appears to be caused by interference with overlapping peaks. The unusually flat trend for peak L is assigned to an M-O-H bending motion. Peaks AD and AE could not be traced to low pressures due to the reduced signal-to-noise ratio of the gasketted, high-pressure runs compared to the ungasketted 1 atm result.

**TABLE 2.** Phase B IR frequencies and Mode Grüneisen parameters

| Type | $\nu_{i0}$ (cm⁻¹) | $\partial\nu/\partial P$ (cm⁻¹/GPa) | $\partial^2\nu/\partial P^2$ (cm⁻¹/GPa²) | $\partial^3\nu/\partial P^3$ (cm⁻¹/GPa³) | $\gamma_{i0}*$ |
|---|---|---|---|---|---|
| O–H | 3631 | 0.365 | | | 0.015 |
| O–H | 3611 | −0.26 | | | −0.01 |
| O–H | 3578 | 0.956 | | | 0.040 |
| O–H | 3561 | 0.877 | | | 0.037 |
| O–H | 3529 | 0.36 | | | 0.015 |
| O20-H1 | 3410.7 | −0.562 | 0.0547 | −0.000847 | −0.025 |
| O21-H2 | 3352.1 | −1.435 | 0.0215 | | −0.064 |
| A† | 1137 | 3.67 | −0.0281 | | 0.48 |
| B† | 1013 | 4.88 | −0.0230 | | 0.72 |
| C‡§ | 987 | 2.899 | | | 0.44 |
| D‡ | 969 | 2.832 | | | 0.44 |
| E‡ | 938 | 2.616 | | | 0.42 |
| F‡ | 922 | 2.809 | | | 0.46 |
| G‡ | 897.4** | 3.08 | | | 0.51 |
| H†† | 877.2** | 4.75 | −0.13 | 0.00267 | 0.81 |
| I§ | 841 | 4.50 | | | 0.80 |
| J§ | 822 | 5.55 | | | 1.01 |
| K§ | 809 | 4.06 | | | 0.75 |
| L‖ | 788 | 1.51 | −0.0263 | | 0.29 |
| M | 729 | 3.28 | | | 0.67 |
| N | 701 | 3.09 | | | 0.66 |
| O | 718.2** | 1.95 | | | 0.41 |
| P | 677 | 2.80 | | | 0.62 |
| Q | 661 | 3.19 | | | 0.72 |
| R | 651 | 3.66 | | | 0.84 |
| S | 623** | 3.49 | | | 0.84 |
| T | 619 | 3.08 | | | 0.75 |
| U | 608 | 2.90 | | | 0.72 |
| V# | 589 | 5.88 | | | 1.50 |
| W# | 582 | 3.53 | −0.0339 | | 0.91 |
| X# | 565 | 4.26 | −0.0500 | | 1.13 |
| Y# | 551.3** | 4.11 | −0.0409 | | 1.12 |
| Z | 546 | 2.68 | | | 0.74 |
| AA# | 525 | 4.32 | −0.0355 | | 1.23 |
| AB | 508.4** | 3.68 | | | 1.09 |
| AC | 503 | 2.88 | | | 0.86 |
| AD | 478 | 2.85 | | | 0.89 |
| AE | 438 | 2.41 | | | 0.83 |

*Notes:* Peaks initially above 1000 cm⁻¹ obtained from the series loaded with liquid Ar as the pressure medium. This sample was too thick to follow most lattice modes. Peaks below 1000 cm⁻¹ were obtained in the set of runs with liquid N₂.
*Uses an estimated $K_T$ = 150 GPa, similar to that of shyB (Pacalo and Weidner 1996).
†Probably O11-Mg stretching.
‡Assigned to stretching of Si tetrahedra.
§Probably stretching of Si octahedra.
‖Assigned to the degenerate Mg-O-H2 bend.
#Probably Mg-O-Mg bending.
**The initial peak position was determined from the least squares fit because these peaks were obscured at 1 atm.
††Fit questionable due to interference (merging and splitting of peaks).

to intensity over all pressures. Several shoulders (those initially at 967, 822, 788, 677, 651, and 589 cm⁻¹) merge with more intense peaks at higher pressure. Other peaks split upon compression (those initially at 882, 701, 546, and 502 cm⁻¹). The splittings can be traced back to 1 atm, showing that this process is related to several accidental degeneracies, ostensibly between the A$_u$ (**E**‖**z**) and

$B_u(\mathbf{E} \mid \mathbf{z})$ symmetries. A significant number of peaks (8 out of 31) merge or split near 22.5 GPa (Table 2, Fig. 2). Only one peak disappears ("C"), probably due solely to its initial weakness and subsequent broadening. At a given pressure, essentially the same spectrum was obtained upon decompression as compression.

IR spectra obtained from the thicker film in Ar (not shown) differ only slightly. Positions from the Ar runs are generally lower than those from the $N_2$ data set, with the discrepancy increasing with pressure (Fig. 2, peaks A, B). The difference is greatest for the weak peak initially at 1013 cm$^{-1}$, probably connected with this being a shoulder on an intense peak that is "offscale" in the Ar runs. For virtually all of the lattice modes, the $N_2$ data set shows a dip from 20 to 22.5 GPa that is neither supported nor refuted by the Ar data set, due to the specific pressures encountered.

Seven of the 31 lattice modes of phase B depend quadratically or cubically on pressure (Table 2). Curvature is discounted for the peak initially at 877 cm$^{-1}$ as it is clearly due to splitting and merging of various bands (Fig. 2).

**ShyB.** Many Raman peaks exist at 1 atm (Fig. 3), but broaden with pressure, allowing only the most intense bands to be tracked reliably. ShyB peak positions depend linearly on pressure (Table 3, Fig. 4).

**Phase A.** Its Raman spectrum at 1 atm (Fig. 3) has 12 intense peaks that can be tracked during compression. Phase A frequencies depend linearly on $P$ (Table 4, Fig. 5).

## Hydroxyl modes

**Phase B.** Peak positions of the intense bands associated with the regular OH sites were obtained from Ar runs (Fig. 6). Frequencies are closely described by a quadratic (for $\nu_{i0} = 3351.2$ cm$^{-1}$) or cubic (for the stronger peak initially at 3410.7 cm$^{-1}$) polynomial in pressure (Fig. 7; Table 2). The initial decrease in $\nu$ for the stronger peak (Fig. 7b) is larger than the uncertainties in $\nu$ and $P$ at low pressure, because the peaks are narrow and the spectral noise is low below 5 GPa. Furthermore, three different loadings of the DAC reproduced $\nu_{i0}$ within 0.2 cm$^{-1}$. $N_2$ runs have similar initial trends (Fig. 7). Minor discrepancies with Ar runs exist at higher pressure, consistent with slight bridging of the diamonds by ruby at high pressure.

The major OH peaks broaden as pressure increases (Fig. 6). FWHM is 12 and 15 cm$^{-1}$ for the 3351 and 3410 cm$^{-1}$ bands, respectively at 1 atm. At 1.90 GPa, FWHM increases to 20 and 25 cm$^{-1}$, and at 37.6 GPa, FWHM is about 43 and 56 cm$^{-1}$. However, intensity increases slightly for the O-H2 band initially at 3352.1 cm$^{-1}$ whereas the area (Figs. 7a and 8) increases substantially and is well described by $A = 115.3 + 2.618\,P - 0.0294\,P^2$ where $P$ is in gigapascals and $A$ is in inverse centimeters. For the O-H1 band at 3410.7 cm$^{-1}$, peak height increases significantly during decompression (Figs. 6 and 8), leading to an area that is closely described by $A = 139.1 + 0.0204\,P + 0.1975\,P^2 - 0.00300\,P^3$. Thus, the same order polynomial applies for $\nu$ and $A$. Parameters from runs in $N_2$ follow similar trends. In contrast, well-resolved lattice modes have constant areas and heights that decrease with $P$ (Fig. 8, bottom), and thus only their widths increase with pressure.

Positions of the weak OH$^-$ peaks depend linearly on pressure (Table 2, Fig. 7a), and are relatively flat lying. Their low intensity precluded accurate measurements of their FWHM, height, and area.

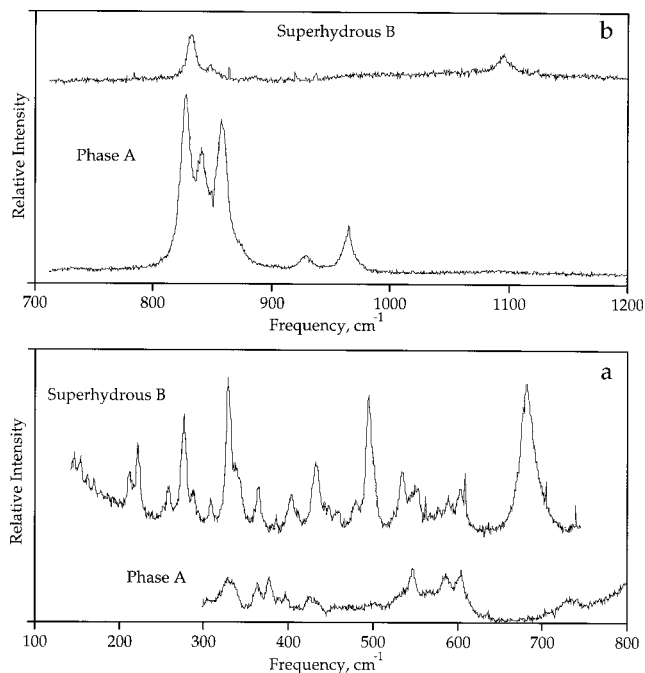**ShyB.** Hydroxyl peak positions from the Raman spectrum of



**FIGURE 3.** Raman spectra of lattice modes of phase A and superhydrous phase B at 1 atm. (**a**) Low-frequency region. (**b**) High-frequency region.

shyB (Fig. 9b) roughly parallel the pressure evolution of the intense OH peaks in phase B (Figs. 7b and 7c). Only a linear dependence on pressure is discernible, due to the narrower pressure range and large sampling intervals. Peak widths for shyB increase with pressure (Fig. 9b). Variation in intensities are not meaningful because of changing sampling site.

**Phase A.** The strong Raman peak for phase A near 3400 cm$^{-1}$

**TABLE 3.** Superhydrous phase B Raman frequencies and Mode Gruneisen parameters

| $\nu_{i0}$ (cm$^{-1}$) | $\partial n/\partial P$ (cm$^{-1}$/GPa) | $\gamma_{i0}$* | Assignment |
|---|---|---|---|
| 3411.8 | 0.56 | 0.025 | O5-H2 |
| 3355.2 | −1.21 | −0.055 | O5-H1(LO) |
| 3349sh | | | O5-H1(TO) |
| 1095.7 | | | O5-Mg stretch |
| 831.6 | 2.90 | 0.54 | SiO$_4$ stretch |
| 681.7 | 2.49 | 0.56 | SiO$_4$ stretch |
| 603.3 | | | Mg-O-Mg? |
| 588.8 | | | |
| 577.2 | | | |
| 534 | 3.78 | 1.09 | Octahedral Si? |
| 494.8 | 2.40 | 0.75 | Octahedral Si? |
| 479.5 | 1.72 | 0.55 | SiO$_4$ bend? |
| 455 | | | |
| 432.2 | | | |
| 405 | | | |
| 365.1 | | | |
| 337 | | | |
| 328.5 | 4.31 | 2.02 | Mg translation |
| 308.7 | | | |
| 288 | | | |
| 276 | 3.19 | 1.78 | Mg translation |
| 258.6 | | | |
| 221.7 | 1.40 | 0.97 | Mg translation |
| 211.9 | | | |

*Uses $K_T$ = 154 GPa (Pacalo and Weidner 1996).

**Table 4.** Raman frequencies and Mode Gruneisen parameters

| Phase A | | | | Chondrite | |
|---|---|---|---|---|---|
| $\nu_{io}$ (cm$^{-1}$) | $\partial\nu/\partial P$ (cm$^{-1}$/GPa) | $\gamma_{io}$* | $\nu_{io}$† (cm$^{-1}$) | $\nu_{io}$‡ (cm$^{-1}$) | Assignment |
| 3615 | | | | | Trace O-H |
| 3579.9 | | | | | Trace O-H |
| 3565§ | 1.52§ | 0.059§ | | 3568 | Chondrodite |
| 3560§ | | | | 3560 | Chondrodite |
| 3535 | | | | | Trace O-H |
| 3518 | 0.31 | 0.013 | 3518 | | O4-H |
| 3401.3‖ | | | 3400 | | O2-H |
| ~3300 | | | | | Trace O-H |
| 965 | 4.69 | 0.70 | ~980 | 967 | SiO$_4$ stretch |
| 929.4 | 2.86 | 0.44 | 894 | 939 | SiO$_4$ stretch |
| 857.5 | 2.61 | 0.44 | 864 | 865 | SiO$_4$ stretch |
| 840.6 | 2.82 | 0.49 | 841 | 843 | SiO$_4$ stretch |
| 826.5 | 2.44 | 0.43 | 799 | 789 | SiO$_4$ stretch |
| 733.5 | | | | 732 | Mg-O-H bend |
| 602.9 | 3.11 | 0.75 | 607 | 605 | Mg-O-Mg ? |
| 587.2 | 1.94 | 0.50 | 567 | 579 | SiO$_4$ bend |
| 547 | 2.27 | 0.60 | 553 | 533 | SiO$_4$ bend |
| | | | 462 | 503 | |
| 424.5 | 4.16 | 1.40 | 433 | | Mg translation |
| 378.5 | 2.79 | 1.07 | 417 | 383 | Mg translation |
| 363.1 | 3.59 | 1.43 | 369 | | Mg translation |
| 328.3 | 2.21 | 0.98 | | 324 | Mg translation |
| | | | 264 | 273 | |
| | | | 227 | | |
| | | | 223 | 221 | |
| | | | 197 | 183 | |
| | | | 179 | 153 | |

*Calculated assuming $K_T$ = 145 GPa (Pawley et al. 1995).
†Raman data of Liu et al. (1997a).
‡Data from Cynn et al. (1996).
§Chondrodite impurities in phase A.
‖This peak disappeared during compression.



**FIGURE 4.** Dependence of Raman lattice modes of shyB on pressure. All lines are linear least-squares fits. Only the intense peaks could be traced reliably; hence data points at low frequency are fewer in number.

at 1 atm was not seen in any of the DAC experiments. This is attributed to orientation of the sample with respect to the O-H vector. Frequencies of the two remaining intense bands (Figs. 7a and 9a) increase linearly with pressure with slopes comparable to those observed for phase B. The doublet near 3560 cm$^{-1}$ arises from chondrodite impurities. Upon decompression, the lower peak that is intrinsic to phase A is observed at 3331 cm$^{-1}$ rather than the 3318 cm$^{-1}$ position measured from the sample external to the cell. This effect is attributed to orientation, because the 3318 cm$^{-1}$ peak has a poorly resolved shoulder at 3335 cm$^{-1}$ at 1 atm (Fig. 9a). Peak widths of OH bands for chondrodite and phase A increase with pressure.

## DISCUSSION

### Comparison with previous data

Our results at 1 atm agree with previous IR and Raman spectra of DHMS (Cynn et al. 1996, and references therein). For all three phases, the distribution of Raman frequencies resembles that of the IR modes, and most Raman peaks lie within 5 cm$^{-1}$ of an IR band (Tables 2–4). Exceptions are discussed below. This behavior is consistent with symmetry analysis (e.g., Table 1), but may involve chance in that these samples have many lattice modes.

**Phase B.** The pressure dependence of the lattice modes not studied previously. For the OH bands, the response of frequency to pressure, resemble previous determinations of Faust and Williams (1996). However, curvature was not previously resolved because their study was non-hydrostatic with poor resolution of the two intense peaks, and used widely spaced pressure intervals, lead-
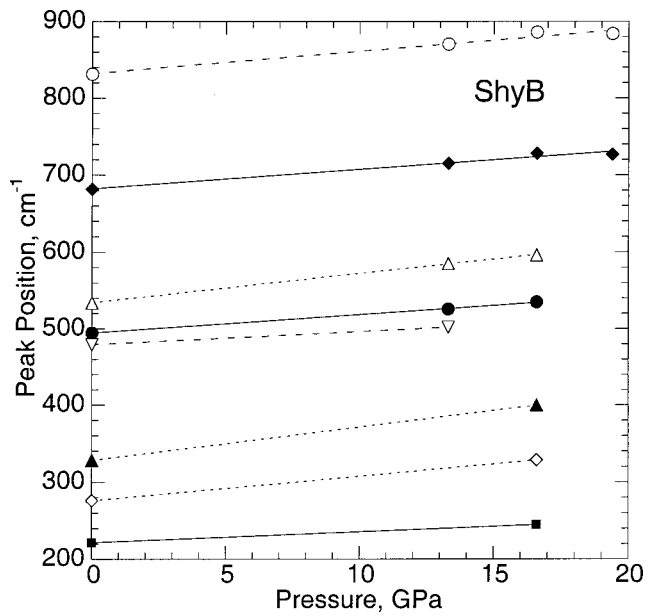
ing to less accurate frequencies. The inference of constant intensity made by Faust and Williams (1996) must be discounted because their peak profiles were initially broad and weak. Their peak profiles could have been affected by water adsorbed in the KBr matrix and/or by the presence of Fe substituting for Mg in their sample.

**ShyB.** Hydroxyl positions from Raman spectroscopy are ~8 cm$^{-1}$ higher than those in the IR, in contrast to differences of a few inverse centimeters for the other samples. If the space group is $P2_1nm$, then the shift results from the selection rules (see "Symmetry Analysis"). This deduction is consistent with a shoulder occurring at the IR position for the lower frequency Raman peak, and the existence of shoulders on the hydroxyl modes for phase A (Fig. 9a), whereas for phase B and chondrodite, LO-TO splitting in the Raman is neither expected nor observed.

**Phase A.** Agreement is fair with the 1 atm Raman data of Liu et al. (1997a). Discrepancies at 1 atm (Table 4) are attributed to sample orientation. This deduction is supported by differences between the spectra of Liu et al. (1997a) at 1 atm and in the DAC.

Minor chondrodite impurities in the phase A sample (Burnley and Navrotsky 1996) are assigned to the doublet ~3660 cm$^{-1}$. Lattice modes of chondrodite are not apparent in the mid-IR at 1 atm, partially because of similarities in frequency due to chemical and structural similarities, and partially because the chondrodite content of the phase A sample is low, about a few percent. The most intense lattice modes of chondrodite could augment the phase A peaks at 841 and 965 cm$^{-1}$. The OH region is sensitive to such minor amounts, because of the greater spread in frequencies and fewer bands: For each DHMS phase, ~40 lattice fundamentals exist between 400 and 1200 cm$^{-1}$, whereas about six O-H stretching fundamentals occur between 3300 and 3700 cm$^{-1}$ (Tables 2 to 4).

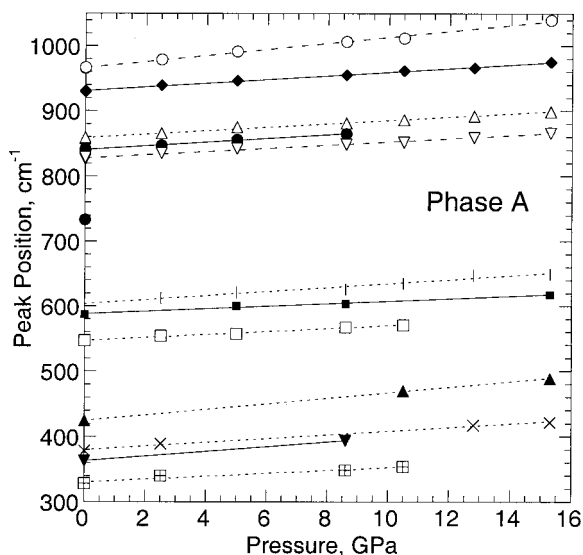The frequencies determined here for phase A depend linearly

**FIGURE 5.** Pressure dependence of the Raman lattice modes of phase A on pressure. All lines are linear least-squares fits.



**FIGURE 6.** Representative near-IR spectra of OH⁻ in phase B from "dry" Ar runs obtained during decompression. Vertical dashes on the 1.9 GPa spectrum indicate trace H in structural defects. The dotted lines on the ~0 GPa spectrum indicate the baselines used in determining peak widths and heights and starting and ending points to obtain areas from integration. Because the ~0 GPa spectrum was collected without a gasket and before compression, its intensity corresponds only roughly with the pressure series. Each spectrum above 1 atm was offset sequentially by 0.4 absorbance units for clarity. The vertical dotted line serves to indicate the initial decrease in $\nu$ for both strong bands.

on $P$ up to the limit of measurements at 16 GPa (Fig. 5), unlike the results of Liu et al. (1997a). Observation of curvature by Liu et al. (1997a) for the lattice modes in phase A below 16 GPa is inconsistent with existing spectroscopic data on silicates, except for his previous study of phase E. First, the degree of curvature is inordinately large. Linear trends are generally seen in Raman spectra acquired below 40 GPa (cf. Chopelas 1990; Kingma et al. 1994), regardless of whether the conditions are hydrostatic or not. The average value of $d^2\nu/dP^2$ of 0.1 cm⁻¹/GPa² reported by Liu et al. (1997a) is a factor of 10 larger than that obtained from the most curved IR peaks for phase B (Table 2). Their values are similar to compliant Mg or Fe translations in IR spectra of olivine (Hofmeister et al. 1989), which itself is much more compressible than DHMS. Second, Liu et al. (1997a) observed curvatures of this order for all lattice modes, whereas linear responses with pressure were observed previously for peaks associated with stretching of the incompressible Si-O tetrahedron (e.g., Hofmeister et al. 1989, Chopelas 1990; Cynn and Hofmeister 1994; Chopelas et al. 1994). The large curvatures in frequency for phases A and E and the inferred phase transitions by Liu et al. (1997a, 1997b) might be due to pressure-induced hydration, as both were compressed in water.

**Phase transition in phase B?**

The gradual and reversible changes in the lattice modes are interpreted as minor structural adjustments, i.e., to decreases in the various bond lengths at different rates. The few discontinuous changes are attributed to accidental degeneracies among the numerous peaks of phase B. The various IR peaks shift at different rates with pressure, and thus combinations of bands move in and out of degeneracy. A smaller number of peaks is seen at high pressure because the peaks are slightly broader and the signal-to-noise ratio is lower. Differential compression is expected for this structure because SiO₄ tetrahedra occur in alternate layers in the structure and because these units are relatively incompressible. The
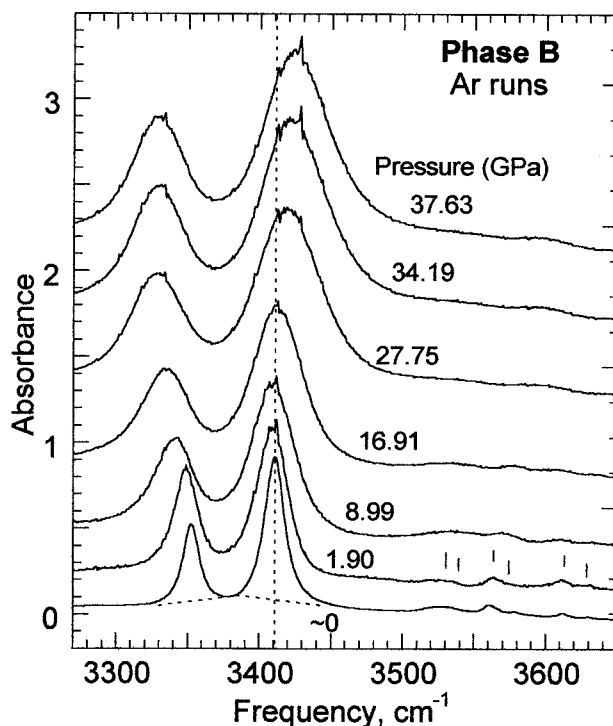
data on phase B suggest that detailed spectra at closely spaced intervals are needed to substantiate phase transitions for low-symmetry structures with many in the unit cell.

**Mode Grüneisen parameters and band assignments for lattice modes**

Particular values of the initial mode Grüneisen parameter, $\gamma_{i0} = (K_T/\nu_{i0})(\partial\nu_i/\partial P)|_0$, where $K_T$ is the bulk modulus at ambient conditions previously have been connected with the different kinds of atomic motions in silicates. As a first approximation, band assignments in Tables 2 to 4 are based on $\nu$, $\gamma_{i0}$, symmetry analysis, and comparisons in the Mg-Si-O-H system. Origins of many modes are uncertain, and mode mixing is likely.

**Configuration of OH in phase B and the importance of the hydrogen bond angle**

Initial frequencies of 3352.1 and 3410.7 cm⁻¹ for phase B imply bond distances of 2.806(3) and 2.859(3) Å, respectively, from the correlation of Mikenda (1986). These are shorter than crystallographic determinations of 2.852 Å for O21-O19 and 2.882 Å for O20-O19 (Finger et al. 1991). The OH...O bonds are slightly
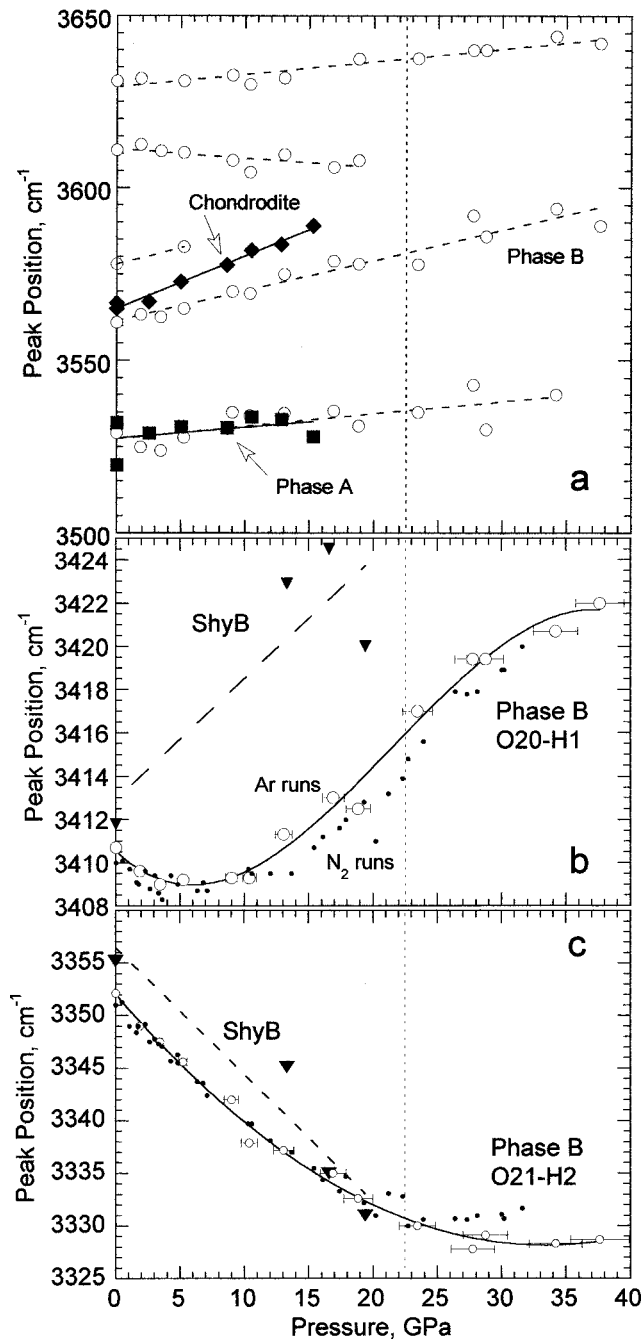
**FIGURE 7.** Pressure dependence of the hydroxyl stretching modes. (**a**) IR data for the weak, defect modes for phase B (open symbols) and for the Raman modes of phase A (filled squares) and chondrodite impurities in phase A (filled circles). Dashed and solid lines are linear least-squares fits (see Tables 2, 3, and 4). (**b** and **c**) Details of intense IR modes of phase B (open circles for runs in Ar, small filled circles for runs in $N_2$) and the Raman modes of shyB (filled triangles). Dashed lines, linear least-squares fits. Solid lines, cubic or quadratic fits for the phase B intense modes. Error bars are indicated for pressure. For frequency, uncertainties are the size of the symbol at low pressure, and slightly larger at high pressure. A possible phase transition at 22.5 GPa is indicated by vertical dotted lines. Vertical scales differ among the three parts.

bent (by 6°) but could be straight, given experimental uncertainties (Finger et al. 1991). Bent bonds of this magnitude are compatible with the observation that weak hydrogen bonds cluster about 170° and 2.7 Å (Steiner and Saenger 1994). NMR data (Phillips et al. 1997) indicate an H-H distance of 1.84(2) Å, which places at least one H atom inside the triangle of O atoms. An O-H bond length equal to the standard neutron diffraction value of 0.96 Å (Chiari and Ferraris 1982) and the NMR constraint yields similar bond angles, and one possibility is shown in Figure 10a. If bond angle is the sole cause of the discrepancy, it would instead increase the OH…O distance over a perfectly linear bond. Possibly, the H-O-M angle influences the hydrogen bonding (Chertanova and Pascard 1996). Most likely, the correlation between $\nu_{OH}$ and OH…O distances (e.g., Mikenda 1986) probably does not hold exactly for phase B because the two H atoms are hydrogen bonded to the same oxygen and thus repulse each other. We assign the 3352 cm⁻¹ band to the shorter bond (H2-O21) because $\nu_{OH}$ always decreases with decreasing O…O distance even though the parameterization of $\nu_{OH}$ with bond length can vary, depending on factors such as metal-oxygen interactions (Beckenkamp and Lutz 1992). Because this hydroxyl has the narrower band, the angle H2-O21-O19 is smaller than the angle H1-O20-O19 for reasons discussed below. The single mid-IR mode that is nearly independent of pressure (Fig. 2) is tentatively attributed to the bending of H2, rather than H1, owing to the parallel curvatures of this bending mode with the 3352 cm⁻¹ band. If H2 bending is degenerate because of the axial symmetry, it should be more intense than H1 bending bands, which were not seen. This comparison suggests an initially linear bond for H2 (Fig. 10a).

Faust and Williams (1996) proposed the opposite assignment, based on crystallographic determinations of O21-H2 and O20-H1 distances. Their assignment is untenable. As discussed by Lutz et al. (1995) and Lutz and Jung (1997), available O-H interatomic distances are inaccurate by an order of magnitude for this purpose, even if based on neutron diffraction.

The pressure dependence (Figs. 7b and 7c) corroborates the location of H1 inside the O20-O19-O21 triangle and of H2 on the edge (Fig. 10a). Pressure drives the more tightly hydrogen-bonded H2 toward O19 along the O21-O19 vector. This bond must approach linearity, or stronger curvature would be seen (Fig. 7). The shortened O21-O19 distance increases the hydrogen bonding and drives the frequency down (Moon and Drickamer 1974; Kruger et al. 1989; Cynn and Hofmeister 1994). For compressions up to 5 GPa, the more weakly hydrogen-bonded H1 also approaches O19 along the O20-O19 vector (Fig. 10a) and its frequency decreases (Figs. 6 and 7b). With further compression, H1 rotates about O21, thus lengthening the H1…O19 bond, and increasing its frequency. [The overturn in frequency near 5 GPa for the more intense band cannot be due to symmetric hydrogen bonds. For such strong bonding in minerals, frequencies near 1000 cm⁻¹ are observed (e.g., Hammer et al. 1998). The hydrogen bonding in phase B remains weak at all pressures.] Because H1 was initially inside the triangle of O atoms, the rotation lies inside the plane of the triangle (Fig. 10) and moves H1 toward O21 above 5 GPa. The initial O21-O20 distance of 3.055 Å is too large for hydrogen bonding to occur. Above 30 GPa, the rise in ν with pressure flattens (Fig. 7b) and at nearly the same high pressure, ν of H2 bottoms out (Fig. 7c). Because ν of the weak OH peaks and most
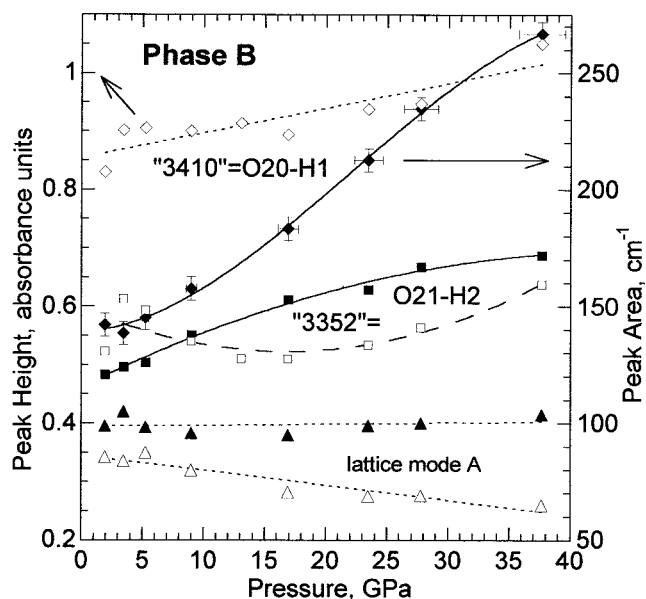
**FIGURE 8.** Peak areas and heights of major near-IR peaks in phase B during decompression in Ar. Data were not collected for this series at 1 atm. Least-squares fits and error bars are shown. Dashed lines, linear fits. Solid lines polynomial fits. Open symbols maximum absorbance (left-hand scale pertains) and filled symbols area obtained by integrating (right-hand scale pertains). Diamonds the peak initially at 3410.7 cm$^{-1}$; squares the peak initially at 3352 cm$^{-1}$.

lattice modes depend linearly on *P* over this range, and the pressure is much less than the bulk modulus of related materials (values discussed below), we infer that flattening results from H configuration rather than resistance of O-O distance to compression. The rotation of H1 shortens the H-H distance (even if the triangle stays the same size). Thus, H-H repulsion forces H2 is out of the triangle (Fig. 10b), and the rotation of H1 slows, presumably due to competing interatomic forces.

Rotation of the sample can be dismissed as causing OH peak heights to increase. The spectra were collected during decompression from a thin film consisting of hundreds of approximately micrometer-sized platelets that was adhered to one diamond. Coordinated rotation of a significant proportion of the crystallites is needed to induce such a change, which is improbable. Changes of the dipole of OH with respect to the crystal lattice due to incoherent rotation would be averaged out. The above discussion and the observation that the lattice modes have constant areas, but heights that decrease with *P* (Fig. 8), indicates that the increases in peak height are intrinsic and that only part of the increases in OH peak width and area are due to pressure gradients.

The increase in area for $\nu_{t0} = 3352.1$ cm$^{-1}$ might be interpreted absolutely from an increase in hydrogen bonding, because Paterson (1982) showed that $A \propto (3780$ cm$^{-1}$-$\nu)$, and thus molar absorption coefficients increase as frequency decreases. However, the magnitude of the change in area (Fig. 8) is larger than expected, and the area of the 3410 cm$^{-1}$ peak increases strongly, opposite to expectations. From these relationships and the ubiquitous broadening of O-H stretching bands with pressure for materials with hydrogen bonding (Moon and Drickamer 1974), we propose that the increase in FWHM with pressure (over that seen for the lattice modes) is due to an increased distribution of OH$\cdots$O angles. Bonds that are initially more bent would be affected more. Peak height increases are connected with increases in FWHM through Maxwell's equations (Wooten 1972).

The association of FWHM with angle is essentially configurational. For a linear complex, there is only one configuration (here, the associated OH...O distance has some spread in values, producing a finite width). For a bent complex, multiple configurations are possible even at 1 atm (the bent bond can vary in orientation), each with the same distribution of OH...O distance. Thus, non-zero angles cause larger peak widths even at 1 atm, as appears to be the case for H1 in phase B, as suggested by its larger initial FWHM that increases with *P*. Width (and thus area) increases with pressure, regardless of bent or linear arrangements for the hydrogen bonding, but more so for a bent bond.

## Determination of bond lengths and angles involving H in phase B

We calculated the crystallographic parameters involving these two H sites using the 1atm frequencies as a calibration. The two H...O19 distances and frequencies at 1 atm (Fig. 10a) define a straight line (not shown). We used trigonometry and assumed that
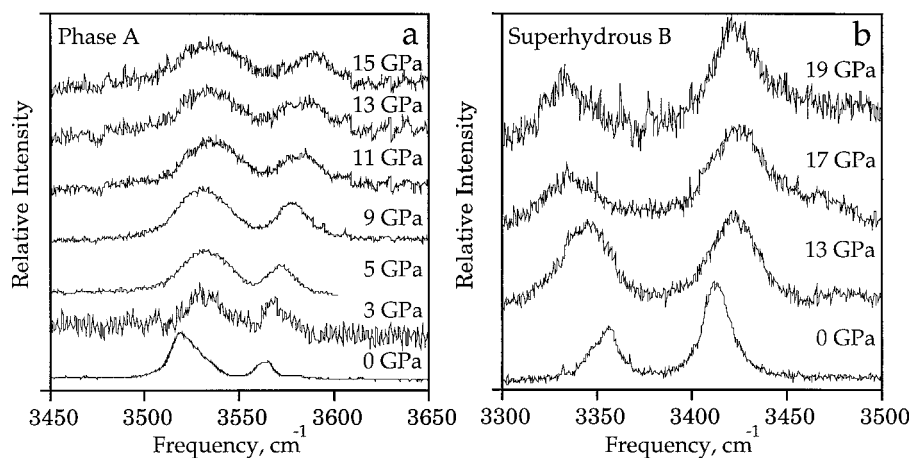


**FIGURE 9.** Raman spectra of the hydroxyl region at pressure. (**a**) Phase A. (**b**) ShyB. Spectra were offset vertically for clarity. Labels are pressures in gigapascals.
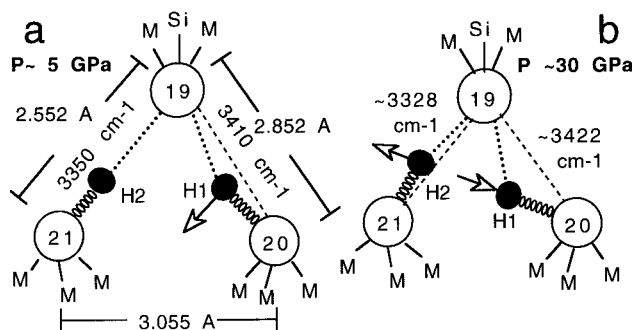
**FIGURE 10.** Schematic illustrations of the H sites in phase B. Open circles = O atoms; coordination with Mg or Si is sketched. Filled circles = H atoms; the "spring" = direct bond; dotted line = the hydrogen bond. Dashed line = the O-O bond for bent configurations. Open arrowheads = motion of H atoms relative to O triangle. (**a**) Proposed arrangement below 5 GPa with parameters from 1 atm. The O-O distances (Finger et al. 1991) are shown for the sides of the triangle. The initial linear decrease in frequency for the 3352 cm$^{-1}$ band implies that this site maintains its linear OH...O configuration at low $P$. The more weakly hydrogen-bonded H1 rotates, thereby reducing the degree of hydrogen bonding and increasing the frequency. (**b**) Arrangement ~30 GPa. Further reduction in the size of the triangle and H-H repulsion forces H2 to the outside. H-H repulsion compresses the H1-O20 bond. H1 rotation is halted because the hydrogen bond is bifurcated.

(1) both initial O-H bond lengths equal the standard neutron diffraction value of 0.96 Å (Chiari and Ferraris 1982); (2) the H2 bond initially is linear (Fig. 10a); (3) the initial compression rate of O20-O19 (before H2 bends) holds up to 40 GPa; and (4) the contraction of O-H bonds can be approximated from the average pressure slope and initial frequency of the trace OH in phase B that lack hydrogen bonding (Fig. 7a). For comparison, calculations were also done with constant O-H distance and with an O-H decrease similar to the rate of change of O-O. A larger range of rates is unlikely for bent bonds and the fairly open sites. The calculated angle for H1 (Fig. 11) increases by $9 \pm 1°$ at 40 GPa, whereas the angle for H2 increases by $11 \pm 1°$. The maximum angle attained by H1 results in H2-H1-O20 being nearly linear, consistent with the inference of H2 being forced out of the triangle of O atoms. The configuration at that point is one of a birfucated hydrogen bond (Fig. 10b). The degree of rotation for H2 roughly maintains the initial H-H distance of 1.84 Å. If a different starting configuration is used, the changes in bond length and angle are similar, although the maximum angles differ. The resulting change in bond distances gives a bulk modulus of ~600 GPa, assuming volume is proportional to length cubed. This high value suggests strong repulsion for O21-O19 and O20-O19, which is not representative of the structure, but is consistent with the local charge distributions. If $K_T \sim 300$ GPa is used, which is appropriate for the tetrahedral layer, then the increase in angle doubles, which is probably not reasonable. This suggests that compression is taken up by the octahedral layer, especially near the Mg atoms.

## OH modes and the space group of shyB revisited

Cynn et al. (1996) suggested that the symmetry of shyB was reduced from *Pnnm* based mainly on the observation of two peaks

in the near IR. Subsequent NMR results by Phillips confirmed the existence of two similar sites for H atoms in shyB and phase B. However, the NMR peaks due to H in shyB were very broad, and only a single NMR peak was seen for Si, the latter observation being consistent with the higher symmetry. The present study shows that hydroxyl groups in shyB behave much the same as in phase B, including the pressure response, corroborating that the environments of the hydroxyls are distinct, but similar. Burnley and Navrotsky (1996) found that the powder XRD pattern of their shyB samples (examined here and by Phillips et al. 1997) matched synthetic patterns generated using the atomic positions of Kudoh et al. (1994) better than those generated from the results of Pacalo and Parise (1992). The lower symmetry space group is a sub-group of *Pnnm*, indicating that a displacive transition is possible between the two. Such differences would be subtle and dependent on the particular distortion. Possibly, local parts of the crystal may exist with ordered placement of H. The breadth of the H peaks could be related to the spatial distribution of the H pairs, and the existence of a singlet peak for Si could result from an "average" structure. Further study is needed.

## Speciation of hydroxyl in phase A and chondrodite

The two sites proposed for hydroxyl in phase A based on the coordination of the O atoms (Horiuchi et al. 1979) are confirmed by our data. The most underbonded site is O2, surrounded by three Mg atoms. The location of H1 on O2 is clearly connected with the 3400 cm$^{-1}$ band: H1 would be hydrogen bonded to O3 and the O2-O3 distance is compatible with the frequency. As pressure increases, the band drops in frequency (Liu et al. 1997a) with a slope close to the initial decrease in the 3410 cm$^{-1}$ band in phase B. This
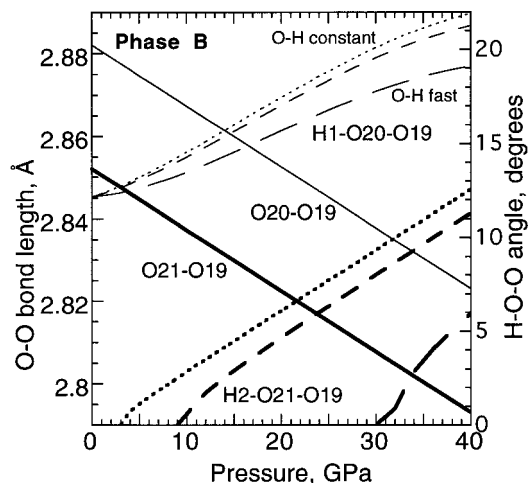


**FIGURE 11.** Dependence of bond parameters involving hydroxyl in phase B on pressure, calculated from the frequencies and O-O bond lengths at 1 atm. Heavy lines, shorter O-O bond involving H2. Light lines, longer O-O bond involving H1. Solid lines, O-O19 distances. Dotted lines, calculated assuming that the O-H distance is unchanged. Dashed lines, calculated assuming that the rate of change of trace hydroxyl applies to the stoichiometric sites. Long dashed lines, rate of change of O-H is four times that of the trace hydroxyl. For H2, the angle is 0° until a minimum pressure is reached. See text for details and Figure 10 for the hydroxyl configuration.

comparison, and the linear frequency response of the phase A band, suggest that H1 is isolated from other H and that the O2H1...O3 bond is nearly linear. The other site is probably the underbonded O4 that is coordinated, but not completely surrounded, by four Mg atoms. The placement is not amenable to hydrogen bonding as the nearest O atoms are fully bonded. The surrounding O atoms lie at 2.934 Å or more, consistent with the frequency of 3518 cm$^{-1}$. The positive pressure shift of the band shows an absence of hydrogen bonding, and is consistent with the approach of the four Mg atoms.

The O-H vectors of the two sites are nearly perpendicular, with the O2-H1 vector lying close to **c**. A basal orientation of our sample in the DAC would explain the absence of the 3400 cm$^{-1}$ band in our high-pressure experiments.

The 3560 cm$^{-1}$ doublet in chondrodite was assigned to an OH that is coordinated triangularly by Mg (Gibbs et al. 1970). This site is not hydrogen bonded because ν increases with $P$ (Fig. 7a), consistent with the approach of the three Mg atoms.

## General relations between $\gamma_{io}$, dν/d$P$, and ν for hydroxyl bands

The pressure derivatives of the hydroxyl bands (Fig. 12) increase nearly linearly with frequency for several different phases. All available literature data are included, excepting a few compounds for which pressure determinations were questionable, and FeOOH. Average slopes of FeOOH are 0 for the peak initially at 3100 cm$^{-1}$ and 3.2 cm$^{-1}$/GPa for the peak at 3200 cm$^{-1}$ (Williams and Guenther 1996). These are not shown because the frequencies are much lower than those of the other compounds and are poorly constrained due to large peak widths. For compressible phases such as micas, analcime, talc, brucite, and portlandite with $K_T$ from 38 to 59 GPa (Hazen and Finger 1979; Meade and Jeanloz 1990; Fei and Mao 1993; Pawley et al. 1995; Comodi and Zanazzi 1995), the trends are steep, whereas for incompressible phases such as phase B and wadsleyite, the trends are shallow. Other DHMS fall roughly on the same trend as phase B, compatible with similar structure and bulk moduli. However, chondrodite, phase A, and shyB with $K_T$ = 136, 145, and 154 GPa, respectively (Faust and Knittle 1994; Pawley et al. 1995; Pacalo and Weidner 1996; Kudoh et al. 1994), have shallower trends than does wadsleyite with $K_T$ = 174 GPa (Weidner et al. 1984). This difference is connected with particular structural arrangements in the DMHS. Location of hydroxyl groups in layers of SiO$_4$ tetrahedra in DHMS suggests that the bulk moduli of O-O bonds being compressed is similar to the polyhedral bulk modulus for $^{IV}$Si of 300 GPa (Hazen and Finger 1982). Thus, the correlation of bulk modulus with the magnitude of the slope of dν/d$P$ against ν (Fig. 12) is consistent with the dependence of frequency on OH...O distances in that interatomic distances change more rapidly with pressure in compressible solids such as micas and hydroxides. This diagram offers a means of inferring bond compressibilities of structurally related materials, given a single-crystal refinement of one substance at high pressure.

The trends for most mineral groups intersect at dν/d$P$ = 0.55 and ν$_{io}$ = 3625 cm$^{-1}$. This frequency lies at the limit of hydrogen bonding, and the positive pressure shift at this frequency is in accord with compression of the O-H bond, in the absence of hydrogen bonding, as the lattice contracts. Larger, more positive shifts

for some cases (Fig. 12) suggest additional cation repulsion, see discussions by Cynn and Hofmeister (1994) and Lutz et al. (1994).

Grüneisen parameters depend similarly on ν, as expected from the definition and the linear dependence of dν/d$P$ on ν. These were not examined here because bulk modulus is unknown for all the solids in Figure 12 and because bond compressibility (unknown for most of these compounds) should actually be used.

## CONCLUSIONS

For hydrous substances, narrow pressure intervals and nearly hydrostatic environments provide details for the response of the OH vibrations with increasing pressure. The relationships allow determination of O-H bond distances and angles from ν($P$), a difficult problem for crystallography. In part, this result follows from the wide spread in OH frequencies as compared with minor changes in the O-H bond length, as discussed by Lutz et al. (1995) and Lutz and Jung (1997), and from the pressure response being indicative of hydrogen-bonding (Lutz et al. 1994). The present data show that not only is the O-O distance important, but also bond angle plays an additional role in hydrogen-bonding, which becomes crucial during compression. Separating these effects (at
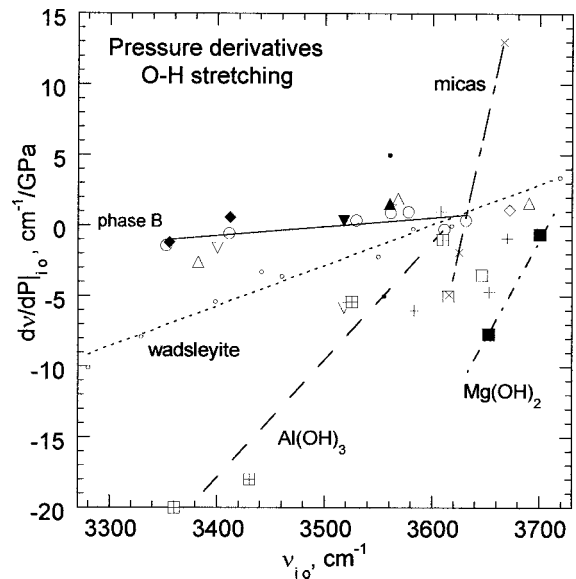


**FIGURE 12.** Correlation of the pressure response dν/d$P$ with ν for the OH bands of hydrous phases. Various lines show linear least-squares fits of OH within a given mineral. Micas were plotted together. The trend for phase B (solid line) also fits the other DHMS. Small open circle = wadsleyite IR (Cynn and Hofmeister 1994). Large open circle = phase B IR (this work). Filled diamond = shyB Raman (this work). Filled downward-pointing triangle = phase A Raman (this work). Open down-pointing triangle = phase A Raman (Liu et al. 1997a). Filled upward-pointing triangle = chondrodite Raman (this work). Open upward-pointing triangle = chondrodite IR (Williams 1992). Open square = portlandite Ca(OH)$_2$ Raman and IR (Meade et al. 1992). Filled square = brucite Mg(OH)$_2$ Raman (Duffy et al. 1995) and IR (Kruger et al. 1989). Square with cross = approximate slopes for gibbsite Al(OH)$_3$ Raman (Huang et al. 1996). Open diamond = talc Raman (Holtz et al. 1993). X = mica Raman (Holtz et al. 1993). Small filled circle = analcime Raman (Velde and Besson 1980). For the latter, pressure is probably not accurate. + = OH in the Si site of garnet (Knittle et al. 1992).

1 atm) will require careful experiments on various hydrogen bonding arrangements as functions of composition, temperature, and pressure.

## REFERENCES CITED

Beckenkamp, K. and Lutz, H.D. (1992) Lattice vibrational spectra Part LXXII. OH stretching frequencies of solid hydroxides—correlation with structural and bonding data. Journal of Molecular Structure, 270, 393–405.

Burnley, P.C. and Navrotsky, A. (1996) Synthesis of high-pressure hydrous magnesium silicates: observations and analysis. American Mineralogist, 81, 317–327.

Chertanova, L. and Pascard, C. (1996) Statistical analysis of noncovalent interactions of anion groups in crystal structures. I. Hydrogen bonding of sulfate anions. Acta Crystallographica, B52, 677–684.

Chiari, G. and Ferraris, G. (1982) The water molecule in crystalline hydrates studied by neutron diffraction. Acta Crystallographica, B38, 2331–2341.

Chopelas, A. (1990) Thermal properties of forsterite at mantle pressures derived from vibrational spectroscopy. Physics and Chemistry of Minerals, 17, 149–156.

Chopelas, A. Boehler, R., and Ko, R. (1994) Thermodynamics and behavior of $\gamma$-$Mg_2SiO_4$ at high pressure and implications for $\gamma$-$Mg_2SiO_4$ phase equilibria. Physics and Chemistry of Minerals, 21, 351–359.

Comodi, P. and Zanazzi, P.F. (1995) High-pressure structural study of muscovite. Physics and Chemistry of Minerals, 22, 170–177.

Cynn, H. and Hofmeister, A.M. (1994) High-pressure IR spectra of lattice modes and OH vibrations in Fe-bearing wadsleyite. Journal of Geophysical Research, 99, 17717–17727.

Cynn, H., Hofmeister, A.M., Burnley, P.C., and Navrotsky, A. (1996) Thermodynamic properties and hydrogen speciation from vibrational spectra of dense hydrous magnesium silicates. Physics and Chemistry of Minerals, 23, 361–376.

Duffy, T.S., Meade, C., Fei, Y., Mao, H.-K., and Hemley, R.J. (1995) High-pressure phase tranistion in brucite, $Mg(OH)_2$. American Mineralogist, 80, 222–230.

Fei, Y. and Mao, H.-K. (1993) Static compression of $Mg(OH)_2$ to 78 GPa at high temperature and constraints on the equation of state of fluid $H_2O$. Journal of Geophysical Research, 98, 11875–11884.

Faust, J. and Knittle, E. (1994) Static compression of chondrodite: implications for water in the upper mantle. Geophysical Research Letters, 21, 1935–1938.

Faust, J. and Williams, Q. (1996) Infrared spectra of phase B at high pressures: hydroxyl bonding under compression. Geophysical Research Letters, 23, 427–430.

Finger, L.W., Hazen, R.M., and Prewitt, C.T. (1991) Crystal structures of $Mg_{12}Si_4O_{19}(OH)_2$ (phase B) and $Mg_{14}Si_5O_{24}$ (phase AnhB). American Mineralogist, 76, 1–7.

Hammer, V.M.F., Libowitzky, E., and Rossman, G.R. (1998) Single-crystal IR spectroscopy of very strong hydrogen bonds in pectolite, $NaCa_2[Si_3O_8(OH)]$, and serandite $NaMn_2[Si_3O_8(OH)]$. American Mineralogist 83, 569–577.

Hazen, R.M. and Finger, L.W. (1979) The crystal structures and compressibilities of layer minerals at high prssures. II. Phlogopite and chlorite. American Mineralogist, 63, 293–296.

———(1982) Comparitive Crystal Chemistry, Wiley-Interscience, New York.

Hofmeister, A.M., Xu, J., Mao, H.K., Bell, P.M., and Hoering, T.C. (1989) Thermodynamics of Fe-Mg olivines at mantle pressures: Mid- and far-infrared spectroscopy at high pressure, American Mineralogist., 74, 281–306.

Holtz, M., Solin, S.A., and Pinnavaia, T.J. (1993) Effect of pressure on the Raman vibrational modes of layered aluminosilicate compounds. Physical Review B48, 13312–13317.

Horiuchi, H., Morimoto, N., Yamamoto, K., and Akimoto, S. (1979) Crystal structure of $2Mg_2SiO_4·3Mg(OH)_2$, a new high-pressure structure type. American Mineralogist, 64, 593–598.

Huang, E., Lin, J.-F., Xu, J., and Yu, S.-C. (1995) Raman spectroscopic study of diaspore up to 25 GPa. Journal of the Geological Society of China, 23, 3083–3086.

Huang, E., Li, A., Xu, J., Chen, R.-J., and Yamanaka, T. (1996) High-pressure phase transition in $Al(OH)_3$: Raman and X-ray observations. Geophysical Research Letters, 23, 3083–3086.

Kauppinen, J.K., Moffatt, D.J., Mantsch, H.H., and Cameron, D.G. (1981) Fourier self-deconvolution: a method for resolving intrinsically overlapped bands. Applied Spectroscopy, 35, 271.

Kingma, K.J., Cohen, R.E., Hemley, R.J., and Mao, H.-K. (1994) Novel signature of post-stishovite silica and implications for the Earth's mantle. Nature, 374, 243–245.

Knittle, E., Hathorne, A., Davis, M., and Williams, Q. (1992) A spectroscopic study of the high-pressure behavior of the $O_4H_4$ substitution in garnet. In Y. Syono and M.H. Manghnani, Eds., High Pressure Research: Application to Earth and Planetary Science, 297–304. Terra Scientific Publishing, Tokyo.

Kruger, M.B., Williams, Q., and Jeanloz, R. (1989) Vibrational spectra of $Mg(OH)_2$ and $Ca(OH)_2$ under pressure. Journal of Chemical Physics, 91, 5910–5915.

Kudoh, Y., Nagase, T., Ohta, S., Sasaki, S., Kanzaki, M., and Tanaka, M. (1994) Crystal structure and compressibility of superhydrous phase B, $Mg_{20}Si_6H_8O_{36}$. In S.C. Schmidt, J.W. Shaner, G.A. Samara, and M. Ross, Eds., High-Pressure Science and Technology-1993, p. 469–472. Gordon and Breach, New York.

Liu, L.-G., Lin, C.-C., Mernagh, T.P., and Irifune, T. (1997a) Raman spectra of phase A at various pressures and temperatures. Journal of the Physics and Chemistry of Solids, 58, 2023–2030.

Liu, L.-G., Mernagh, T.P., Lin, C.-C., and Irifune, T. (1997b) Raman spectra of phase E at various pressures and temperatures with geophysical implications. Earth and Planetary Science Letters, 149, 57–65.

Luth, R.W. (1993) Volatile-bearing phases in the Earth's mantle. In Short Course Handbook, 21, p. 445-485.

Lutz, H.D. and Jung, C. (1997) Water molecules and hydroxide ions in condensed materials: correlation of spectroscopic and structural data. Journal of Molecular Structure, 404, 63–66.

Lutz, H.D., Bechenkamp, K., and Möller, H. (1994) Weak hydrogen bonds in solid hydroxides and hydrates. Journal of Molecular Structure, 322, 263–266.

Lutz, H.D., Jung, C., Trömel, M., and Lösel, J. (1995) Brown's bond valences, a measure of the strength of hydrogen bonds. Journal of Molecular Structure, 351, 205–209.

Meade, C. and Jeanloz, R. (1990) Static compression of $Ca(OH)_2$ at room temperature: observations of amorphization and equation of state measurements to 10.7 GPa. Geophysical Research Letters, 17, 1157–1160.

Meade, C., Jeanloz, R., and Hemley, R.J. (1992) Spectroscopic and X-ray studies of metastable crystalline-amorphous transition in $Ca(OH)_2$ and serpentine, p. 485–492. Terra Scientific Publishing, Tokyo.

Mikenda, W. (1986) Stretching frequency versus bond distance correlation of O-D(H)...Y (Y=N, O, S, Se, Cl, Br, I) hydrogen bonds in solid hydrates. Journal of Molecular Structure, 147, 1–15.

Moon, S.H. and Drickamer, H.G. (1974) Journal of Chemical Physics, 61, 48.

Pacalo, R.E.G. and Parise, J.B. (1992) Crystal structure of superhydrous B, a hydrous magnesium silicate synthesized at 1400 °C and 20 GPa. American Mineralogist, 77, 681–684.

Pacalo, R.E.G. and Weidner, D.J. (1996) Elasticity of superhydrous B. Physics and Chemistry of Minerals, 23, 520–525.

Pawley, A.R., Redfern, S.A.T., and Wood, B.J. (1995) Thermal expansivities and compressibilities of hydrous phases in the system $MgO-SiO_2-H_2O$: talc, phase A, and 10-Å phase. Contributions to Mineralogy and Petrology, 122, 301–307.

Paterson, M.S. (1982) The determination of hydroxyl by infrared absorption in quartz, silicate glasses and similar minerals. Bulletin de Mineralogie 105, 20–29.

Phillips, B.L., Burnley, P.C., Worminghaus, K., and Navrotsky, A. (1997) $^{29}Si$ and $^1H$ NMR spectroscopy of high-pressure hydrous magnesium silicates. Physics and Chemistry of Minerals, 24, 179–190.

Prewitt, C. and Finger, L.W. (1992) Crystal chemistry of high-pressure hydrous magnesium silicates. In Y. Syono and M.H. Manghnani, Eds., High Pressure Research: Application to Earth and Planetary Science, p. 269–274. Terra Scientific Publishing, Tokyo.

Scott, J.F. and Porto, S.P.S. (1967) Longitudinal and transverse optical lattice vibrations in quartz. Physical Review, 161, 903–910.

Steiner, T. and Saenger, W. (1994) Lengthening of the covalent O-H bond in O-H···O hydrogen bonds re-examined from low-temperature neutron diffraction data of organic compounds. Acta Crystallographica, B50, 348–357.

Velde, B. and Besson, J.M. (1981) Raman spectra of analcime under pressure. Physics and Chemistry of Minerals, 7, 96–99.

Weidner, D.J., Sawamoto, H., Sasaki, S., and Kumazawa, M. (1984) Single crystal elastic properties of the spinel phase $Mg_2SiO_4$. Journal of Geophysical Research, 89, 7852–7860.

Williams, Q. (1992) Vibrational spectroscopic study of hydrogen in high pressure minerals assemblages. In Y. Syono and M.H. Manghnani, Eds., High Pressure Research: Application to Earth and Planetary Science, p. 289-296. Terra Scientific Publishing, Tokyo.

Williams, Q. and Guenther, L. (1996) Pressure-induced changes in the bonding and orientation of hydrogen in FeOOH-goethite. Solid State Communications, 100, 105–108.

Wooten, F. (1972) Optical properties of solids. Academic, San Diego.